Order-to-Order Transitions of Block Copolymer in Film Geometry

Changhak Shin,[†] Du Yeol Ryu,*[,†] June Huh,[†] Jung Hyun Kim,[†] and Kwang-Woo Kim[‡]

Department of Chemical Engineering, and Active Polymer Center for Pattern Integration, Yonsei University, Seoul 120-749, Korea, and Pohang Accelerator Laboratory, Pohang 790-784, Korea

Received December 8, 2008; Revised Manuscript Received February 3, 2009

ABSTRACT: The various mesophasic transitions for an asymmetric polystyrene-*block*-polyisoprene (PS-*b*-PI) in film geometry, like the order-to-order transitions, were investigated by *in situ* grazing incidence small-angle X-ray scattering (GISAXS). Compared with the sequential phase transitions in bulk, lamella (LAM) to hexagonally perforated layer (HPL) to gyroid (GYR) to hexagonally packed cylinder (HEX) to disorder (DIS) by thermal energy, the only difference in geometry leads to the enhancement of LAM phase, the parallel shifts of transition temperatures for HPL and GYR phases, and a little increase of order-to-disorder temperature (T_{ODT}) as a consequence of weak interfacial interactions. However, a short-range of HEX phase in bulk disappears. These results may be correlated to the suppressed compositional fluctuation in film geometry due to the interactions of polyisoprene block with the substrate and air.

Introduction

Periodic self-assembled morphologies of block copolymers (BCPs) have recently attracted significant interest as fascinating candidates in applications of nanoscopic patterns in thin film.[1−5] When χN is sufficiently large where χ and N are the segmental interaction parameter and the total number of segments in the BCP, in principle, the microphase separation occurs in tens of nanometers depending on the volume fraction of each component;[6−15] thereby producing lamellar (LAM), hexagonally packed cylindrical (HEX), body centered cubic spherical (BCC), and the complex phases such as gyroid (GYR) and hexagonally perforated layers (HPL) which has been believed a metastable phase.[10,15,16] Hence, it is a key issue to control morphologies in the BCP films, particularly in the directed microdomain orientations.

Of the various BCPs, a polystyrene-*block*-polyisoprene (PS-*b*-PI) has been used as a model system to illustrate the phase behaviors consisting of a variety of ordered structures, which provide us with the intriguing phase transitions by thermal energy at specific composition regime within volume fraction of 0.6−0.7 due to strong temperature dependence on χ.[17−19] These transitions of BCP, namely order-to-order transitions (OOT), can be speculated by the mean field approach in a relatively good agreement with the experimental results.[20,21] In addition, a new noncubic network (*Fddd*) phase for PS-*b*-PI was recently found in a narrow range of the volume fraction and χN.[22]

For the film geometry, interfacial interactions at the substrate/polymer and polymer/air play a key role in understanding the phase behaviors of BCP since they affect the relative stability of mesophases as well as the microdomain orientations by the preferential interaction.[23,24] Nevertheless, there has been no straightforward report experimentally on mesophasic (or order-to-order) transitions in BCP films, with them being an open question. Grazing incidence small-angle X-ray scattering (GISAXS) measurement has recently provided the detailed analysis for the BCP films through the characteristic patterns to the corresponding nanostructures, where the target depth of films can be tuned by varying the incident angles.[25−29] As a part of regulating these interactions, we previously reported through GISAXS measurement for symmetric PS-*b*-PI films that the preferential interactions by PS brushes with one component of the BCP can lead to enhanced orientation of the symmetric lamellar microdomain parallel to the film surface and a shift of the order-to-disorder temperature (T_{ODT}) as a consequence of an amplification of the periodic composition.[30]

In this study, we report the phase transition behavior for a PS-*b*-PI in film geometry by *in situ* GISAXS in comparison to the bulk phase behavior composed of LAM−HPL−GYR−HEX−DIS, as a new approach to the confinement effect for transition behavior of BCP. The only difference in geometry with no significant surface modification could lead to the changes and shifts of transition temperatures more than likely because interfacial interactions in film geometry are key factors in determining the phase stability. To the best of our knowledge, there has been no report on OOT behaviors of BCP films by thermal energy in comparison to those of bulk, even though the structure analysis for complex morphologies of thick films was well-described.[25,26,31] Therefore, this report will stimulate a new study regarding transition behavior in BCP films by controlling the strength of the surface interactions as the next study.

Experimental Section

An asymmetric BCP composed of styrene and isoprene, hereafter denoted to as SI-42, was synthesized by the sequential anionic polymerization in cyclohexane at 45 °C under purified argon using *sec*-butyllithium as an initiator. The number-average molecular weight (M_n) and polydispersity index (PDI), characterized by size-exclusion chromatography (SEC), was measured to be 42 400 g/mol and 1.04, respectively. PS volume fraction (Φ_{PS}) of BCP was determined to be 0.333 by ^{1}H nuclear magnetic resonance (^{1}H NMR) based on the mass densities of two components (1.05 and 0.90 g/cm^3 for PS and PI). A given amount of SI-42 was dissolved in toluene and spin-coated onto the standard Si substrate, where the substrate was cleaned with toluene and dried with a stream of nitrogen before use. Subsequently, the BCP films were annealed at 90 °C under vacuum for 48 h to allow thermal equilibrium between T_g (75 °C) of PS block and the first OOT temperature (T_{OOT}). The film thickness measured by ellipsometry was set to be approximately 960 nm, which is consistent with $40L_0$ by $d = 2\pi/q^*$.

Synchrotron scattering experiments were conducted at 4C1 (SAXS) and 4C2 (GISAXS) beam-lines of the Pohang Accelerator Laboratory (PAL), Korea.[32] The operating conditions for GISAXS

* To whom correspondence should be addressed. E-mail dyryu@yonsei.ac.kr.
[†] Department of Chemical Engineering, and Active Polymer Center for Pattern Integration, Yonsei University.
[‡] Pohang Accelerator Laboratory.

10.1021/ma802737s CCC: $40.75
Published on Web 02/24/2009

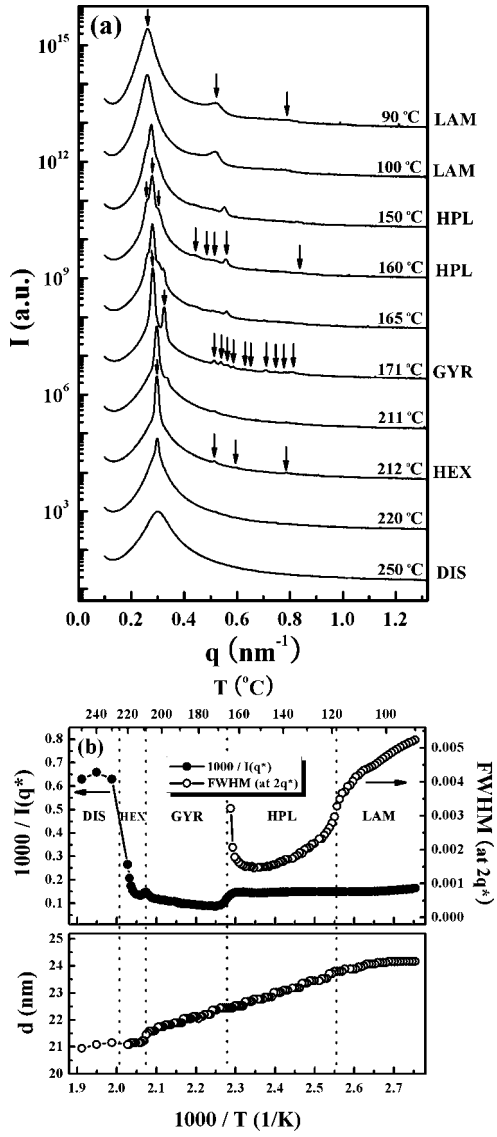

Figure 1. (a) SAXS intensity profiles for bulk SI-42 as a function of scattering vector (q) at various temperatures ranging from 90 to 250 °C at a heating rate of 0.9 °C/min, and (b) the scattering parameters derived from SAXS profiles. The inverse of the maximum intensity ($1/I(q^*)$), full-width at half-maximum (fwhm) at $2q^*$, and d-spacing (d) by $d = 2\pi/q^*$ are plotted as a function of inverse temperature (1/K).

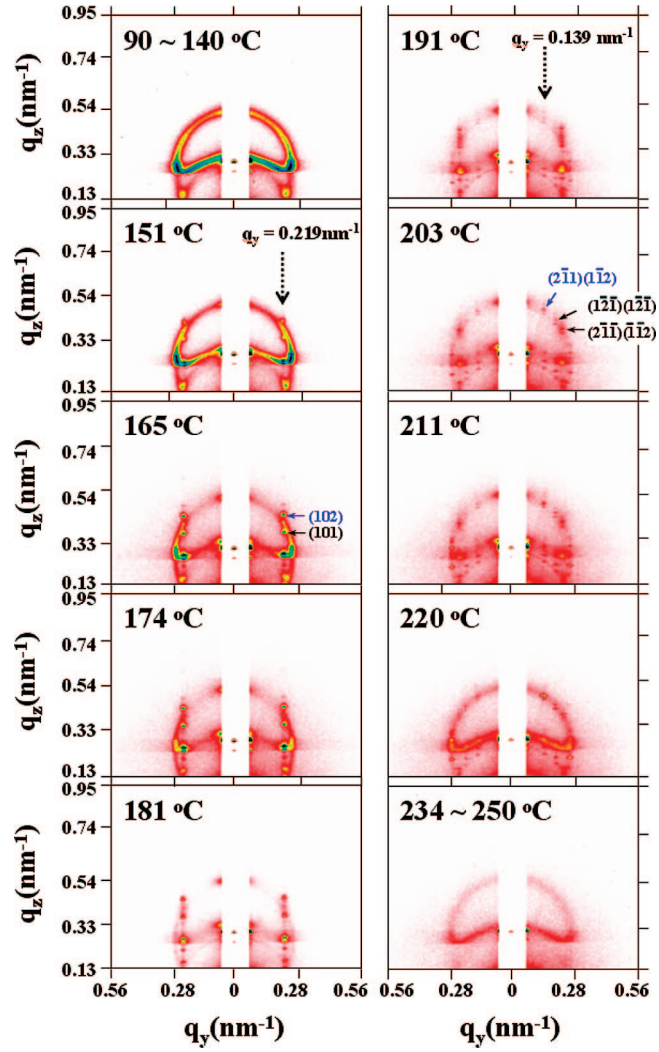

Figure 2. 2D GISAXS patterns for the film of 962 ± 11 nm ($40L_0$) on Si substrate at incident angle of 0.18°, which is above the critical angle for SI copolymer (0.15°). All patterns were taken during heating from 90 to 250 °C at a heating rate of 0.9 °C/min after thermally annealing thin film at 90 °C for 48 h under vacuum. The dotted arrows indicate the characteristic lines to determine HPL and GYR phases at constant $q_y = 0.219$ nm^{-1} and $q_y = 0.139$ nm^{-1}, respectively.

were set to a wavelength of 1.38 Å and the sample-to-detector distance of 2.3 m. The film samples were mounted on a heating cell under vacuum and the incident angle was set at 0.18°, which is above the critical angle (0.15°) of BCP thin films.[26] 2D GISAXS patterns were recorded using a CCD detector (Princeton Instruments) positioned at the end of a vacuum guide tube when the X-ray beam pass through the BCP films under vacuum. SAXS was used to determine the bulk behavior of the BCP. All the heating experiments were automatically controlled with a PID temperature controller from 80 to 250 °C at constant heating rate of 0.9 °C/min and with an exposure time of 60−120 s.

Results and Discussion

Figure 1a shows SAXS intensity profiles as a function of the scattering vector (q), reflecting the phase structures in bulk SI-42, which were measured by 2D SAXS patterns at various temperatures during heating, where $q = (4\pi/\lambda)[\sin\theta]$, 2θ and λ are the scattering angle and wavelength, respectively. The ordered structure at lower temperatures ($T \leq 100$ °C) corresponds to LAM phase, which is evidenced by a sharp scattering peak and the higher-order peaks (indicated by arrows) at scattering vector ratios of $q/q^* = 1{:}2{:}3$ relative to a primary peak located at q^* (at maximum). As temperature increases ($T > 125$ °C), the primary peak begins to change due to the appearance of shoulders at both sides and all peaks divide into eight different peaks at $q/q^{first} = 1{:}1.09{:}1.18{:}1.73{:}1.90{:}2.0{:}2.18{:}3.27$, as shown in the intensity profile at 160 °C, where q^{first} indicates the scattering vector at the first peak.[15,16] This is in good agreement with the HPL phase in the A−B−C stacking pattern. With further increasing temperatures ($T > 165$ °C), through a transition at 165 °C, the intensity profile observed at 171 °C shows two sharp peaks at $q/q^* = \sqrt{3}{:}\sqrt{4}$ and the series of higher-order peaks at $q/q^* = \sqrt{10}{:}\sqrt{11}{:}\sqrt{12}{:}\sqrt{13}{:}\sqrt{15}{:}\sqrt{16}{:}\sqrt{19}{:}\sqrt{21}{:}\sqrt{23}{:}\sqrt{25}$, which are characteristics of GYR phase.[9,11,15] For the intensity profile at 212 °C, the next phase structure upon heating corresponds to HEX phase, consistent with the scattering vector ratios of $q/q^* = 1{:}\sqrt{3}{:}\sqrt{4}{:}\sqrt{7}$. At higher temperature for $T > 225$ °C, the primary peak weakens and broadens abruptly and the higher-order peaks disappear, indicating the correlation hole scattering of a phase-mixed (or disordered) BCP in bulk.

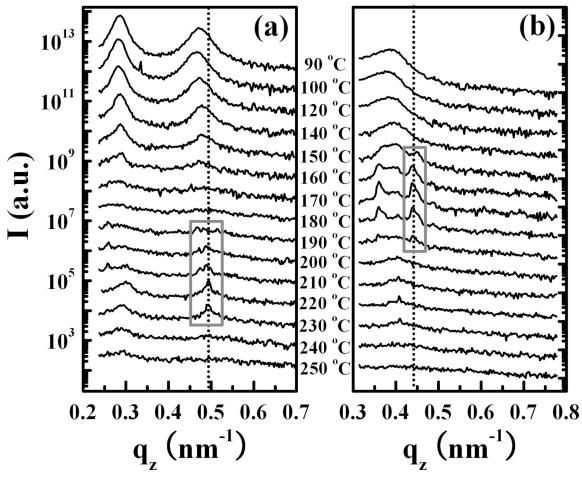

Figure 3. *Out-of-plane* scattering intensities scanned along q_z-direction from GISAXS patterns for SI-42 (a) at constant $q_y = 0.139$ nm^{-1}, which can provide information on the characteristic GYR phase at the peak at $(2\bar{1}1)(1\bar{1}2)$, and (b) at constant $q_y = 0.219$ nm^{-1} involving the two distinct peaks at (102) and (101) from the reflected X-ray beam, indicative of HPL phase.

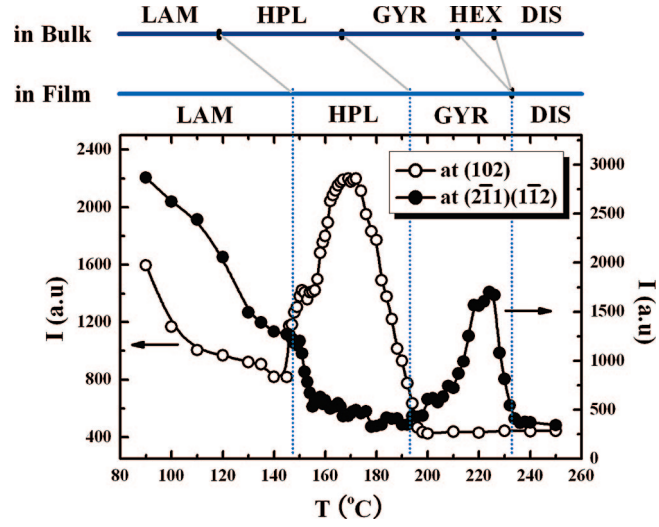

Figure 4. Maximum peak intensities at positions of (102) and $(2\bar{1}1)(1\bar{1}2)$, as indicated by the dotted lines in Figure 3 (or the blue color in Figure 2). The transition temperatures in film geometry are determined by the significant changes in intensities and confirmed by the GISAXS patterns, leading to the order-to-order transition temperatures (T_{OOT}'s) divided by the dotted lines. On the top of figure, transition temperature window in film geometry is compared with that in bulk.

For more accurate information, temperature dependences of the scattering parameters such as the inverse of the maximum intensity (1/I(q*)), full-width at half-maximum (fwhm) and *d*-spacing (*d*) by $d = 2\pi/q^*$ are plotted in Figure 1b as a function of inverse temperature (1/K). Especially for the first transition from LAM to HPL ($T < 164$ °C), fwhm at $2q^*$ was analyzed because $1/I(q^*)$ is unmeaningful for this transition, consequently leading to a broad transition of $T_{OOT} = 118 \pm 6$ °C. By the sequentially discontinuous changes of $1/I(q^*)$, one can readily determine further transition temperatures from HPL to GYR at $T_{OOT} = 165 \pm 3$ °C, GYR to HEX at $T_{OOT} = 211$ °C, and disordering (DIS) at $T_{ODT} \approx 225$ °C, respectively. The *d*-spacing decreases gradually with increasing temperature although it shows some weak variations at each transition. This behavior is characteristic for BCPs undergoing the sequential phase transitions, LAM-HPL-GYR-HEX-DIS by thermal energy, which will be compared to that in the films presented in Figure 4.

In comparison to the phase transitions for the bulk SI-42, Figure 2 shows 2D GISAXS patterns for the film of 962 ± 11 nm, which were taken at each temperature during heating after thermally annealing thin film on Si substrate at 90 °C for 48 h under vacuum. In order to avoid the film thickness dependence on transitions under quasi-equilibrium which is responsible for the influence of the surface interactions, this thickness was set to $\sim 40L_0$ at which L_0 is consistent with *d*-spacing (L_0 or $d = 2\pi/q^*$) of 24.0 nm at a low temperature of 90 °C for lamella-forming range. In the scattering geometry, q_y is the scattering vector normal to the incident plane where *d*-spacing is related to q_y by $d = 2\pi/q_y$, and q_z is the scattering vector normal to the sample surface, defined as $q_z = (4\pi/\lambda)[\sin\theta]$. The incident angle ($\alpha_i$) was set at 0.18° to probe the internal structures of the entire film when the X-rays pass through the thin film above the critical angle ($\alpha_c = 0.15°$) of SI-42.

For $T = 90-140$ °C the GISAXS pattern shows two intensified elliptical patterns arising from a superposition of the two scatterings from the reflected and transmitted X-ray beams by the difference of $2\alpha_i$, which is caused by the random orientation of LAM microdomains. It should be also mentioned that in bulk a HPL phase was observed even at $T = 140$ °C, indicating that a transition from LAM to HPL is shifted to higher temperature in film on the native oxide layer of Si substrate. The favorable random orientation at the extended temperature range for LAM phase in film geometry can be attributed to the asymmetric composition for SI-42($\Phi_{PS} = 0.333$) in addition to the weak interactions between oxide layer and polyisoprene block.

As temperature increases over $T = 150$ °C, a characteristic A−B−C stacking HPL pattern appear periodically at the *out-of-plane* scattering peaks along the q_z-direction (as indicated at $q_y = 0.219$ nm^{-1}) at the expense of the elliptical patterns from LAM phase. According to the peak indexes for HPL phase,[25,28,29] a number of periodic scattering peaks from the reflected and transmitted X-ray beams indicate that most lattice layers are oriented parallel to the film surface, which is contrast to the random orientation of LAM microdomains. These scattering patterns and peaks enhance up to $T = 174$ °C but weakens at $T = 181$ °C, maintaining the same morphology. For $T = 191$ °C, the new *out-of-plane* scattering peaks begin to appear along q_z-direction (as indicated at $q_y = 0.139$ nm^{-1}) and the marked scattering peaks at {121} plane remain arranged distinctly at $T = 203-220$ °C, which correspond to GYR phase having a little preferential orientation in film geometry.[25−27] However, HEX phase in bulk for $T = 212-220$ °C was not observed in thin film. Finally for $T > 234$ °C with further increasing temperature, all characteristic peaks disappear and two broader elliptical scattering patterns appear, which should be attributed to the correlation hole scattering from a disordered BCP in film geometry.

For better statistics, we analyzed two *out-of-plane* scattering intensities involving the characteristic peaks for HPL and GYR phases, as highlighted by a square in Figure 3, where the intensities were scanned along the q_z-direction at constant $q_y = 0.139$ and 0.219 nm^{-1} from the GISAXS patterns in Figure 2. Figure 3a shows the intensity profiles at $q_y = 0.139$ nm^{-1}, which can provide information on the characteristic GYR phase at the peak at $(2\bar{1}1)(1\bar{1}2)$. However, for $q_y = 0.219$ nm^{-1} in Figure 3b, the intensity profiles include the intensity changes involving the two distinct peaks at (102) and (101) from the reflected X-ray beam, which are indicative of the HPL phase. Hence, these results allow us to follow the structural changes in film geometry of $40L_0$ during heating, which are reasonably consistent with the direct analysis of the GISAXS patterns.

Figure 4 shows a summary of scattering intensities at positions of (102) for HPL and $(2\bar{1}1)(1\bar{1}2)$ for GYR phase, as indicated

by the dotted lines in Figure 3 (or the blue color in Figure 2). The order-to-order transition temperatures (T_{OOT}'s) in film geometry are determined by the significant changes in intensities and confirmed by the GISAXS patterns, resulting in LAM to HPL at $T_{OOT} = 148 \pm 3$ °C, HPL to GYR at $T_{OOT} = 193 \pm 2$ °C, and disordering (DIS) transition at $T_{ODT} = 232$ °C with no evidence for HEX phase, respectively. Moreover, the maxima of intensities by thermal energy in Figure 4 represent that the transition behaviors in film are slower than those in bulk. The sequential phase transitions in bulk, LAM−HPL−GYR−HEX−DIS, are plotted on top of Figure 4 for comparison. For the film geometry, the only weak interfacial interactions from two interfaces at the native oxide/polyisoprene block and polyisoprene block /air lead to the enhancement of LAM phase, the parallel shifts of transition temperatures (T_{OOT}'s) for HPL and GYR phases, and a little increase of T_{ODT}. These results may be correlated to the suppressed compositional fluctuation due to the interactions of polyisoprene block with the substrate and air. A short-range of HEX phase in bulk, however, disappears in film, representing that the phase stability in film geometry can also be readily influenced by the interfacial interactions. Therefore, it is of great interest to investigate the surface field effects on OOT of BCP in film as a further study.

Acknowledgment. This work was supported by a Korea Research Foundation Grant (KRF-2008- D00297), the APCPI ERC program (R11-2007-050-01004) funded by the Ministry of Education, Science & Technology (MEST), and the Seoul Research and Business Development Program (10816 ICBIN), Korea.

References and Notes

(1) Hamley, I. W. *Nanotechnology* **2003**, *14*, R39.
(2) Hawker, C. J.; Russell, T. P. *MRS Bull* **2005**, *30*, 952.
(3) Stoykovich, M. P.; Nealey, P. F. *Mater. Today* **2006**, *9*, 20–29.
(4) Black, C. T. *ACS Nano* **2007**, *1*, 147–150.
(5) Tang, C.; Lennon, E. M.; Fredrickson, G. H.; Kramer, E. J.; Hawker, C. J. *Science* **2008**, *322*, 429–432.
(6) Leibler, L. *Macromolecules* **1980**, *13*, 1602–1617.
(7) Fredrickson, G. H.; Bates, F. S. *Annu. Rev. Mater. Sci.* **1996**, *26*, 501–550.
(8) Hamley, I. W.; Castelletto, V. *Prog. Polym. Sci.* **2004**, *29*, 909–948.
(9) Hajduk, D. A.; Harper, P. E.; Gruner, S. M.; Honeker, C. C.; Kim, G.; Thomas, E. L.; Fetters, L. J. *Macromolecules* **1994**, *27*, 4063–4075.
(10) Foerster, S.; Khandpur, A. K.; Zhao, J.; Bates, F. S.; Hamley, I. W.; Ryan, A. J.; Bras, W. *Macromolecules* **1994**, *27*, 6922–6935.
(11) Vigild, M. E.; Almdal, K.; Mortensen, K.; Hamley, I. W.; Fairclough, J. P. A.; Ryan, A. J. *Macromolecules* **1998**, *31*, 5702–5716.
(12) Qi, S.; Wang, Z. G. *Macromolecules* **1997**, *30*, 4491–4497.
(13) Park, M. J.; Nedoma, A. J.; Geissler, P. L.; Balsara, N. P.; Jackson, A.; Cookson, D. *Macromolecules* **2008**, *41*, 2271–2277.
(14) Hiroshi, Jinnai; Hasegawa, H.; Nishikawa, Y.; Sevink, G. J. A.; Braunfeld, M. B.; Agard, D. A.; Spontak, R. J. *Macromol. Rapid Commun.* **2006**, *27*, 1424–1429.
(15) Zhu, L.; Huang, P.; Chen, W. Y.; Weng, X.; Cheng, S. Z. D.; Ge, Q.; Quirk, R. P.; Senador, T.; Shaw, M. T.; Thomas, E. L.; Lotz, B.; Hsiao, B. S.; Yeh, F.; Liu, L. *Macromolecules* **2003**, *36*, 3180–3188.
(16) Ahn, J. H.; Zin, W. C. *Macromolecules* **2000**, *33*, 641–644.
(17) Khandpur, A. K.; Foerster, S.; Bates, F. S.; Hamley, I. W.; Ryan, A. J.; Bras, W.; Almdal, K.; Mortensen, K. *Macromolecules* **1995**, *28*, 8796–8806.
(18) Zhao, J.; Majumdar, B.; Schulz, M. F.; Bates, F. S.; Almdal, K.; Mortensen, K.; Hajduk, D. A.; Gruner, S. M. *Macromolecules* **1996**, *29*, 1204–1215.
(19) Schulz, M. F.; Khandpur, A. K.; Bates, F. S.; Almdal, K.; Mortensen, K.; Hajduk, D. A.; Gruner, S. M. *Macromolecules* **1996**, *29*, 2857–2867.
(20) Matsen, M. W.; Schick, M. *Phys. Rev. Lett.* **1994**, *72*, 2660.
(21) Matsen, M. W.; Bates, F. S. *Macromolecules* **1996**, *29*, 1091–1098.
(22) Takenaka, M.; Wakada, T.; Akasaka, S.; Nishitsuji, S.; Saijo, K.; Shimizu, H.; Kim, M. I.; Hasegawa, H. *Macromolecules* **2007**, *40*, 4399–4402.
(23) Anastasiadis, S. H.; Russell, T. P.; Satija, S. K.; Majkrzak, C. F. *Phys. Rev. Lett.* **1989**, *62*, 1852.
(24) Anastasiadis, S. H.; Russell, T. P.; Satija, S. K.; Majkrzak, C. F. *J. Chem. Phys.* **1990**, *92*, 5677–5691.
(25) Lee, B.; Park, I.; Park, S.; Yoon, J.; Kim, J.; Kim, K. W.; Chang, T.; Ree, M. *Macromolecules* **2005**, *38*, 4311–4323.
(26) Park, I.; Lee, B.; Ryu, J.; Im, K.; Yoon, J.; Ree, M.; Chang, T. *Macromolecules* **2005**, *38*, 10532–10536.
(27) Jin, S.; Yoon, J.; Heo, K.; Park, H.-W.; Kim, J.; Kim, K.-W.; Shin, T. J.; Chang, T.; Ree, M. *J. Appl. Crystallogr.* **2007**, *40*, 950–958.
(28) Lee, B.; Park, I.; Park, H.; Lo, C.-T.; Chang, T.; Winans, R. E. *J. Appl. Crystallogr.* **2007**, *40*, 496–504.
(29) Heo, K.; Yoon, J.; Jin, S.; Kim, J.; Kim, K.-W.; Shin, T. J.; Chung, B.; Chang, T.; Ree, M. *J. Appl. Crystallogr.* **2008**, *41*, 281–291.
(30) Shin, C.; Ahn, H.; Kim, E.; Ryu, D. Y.; Huh, J.; Kim, K. W.; Russell, T. P. *Macromolecules* **2008**, *41*, 9140–9145.
(31) Park, H. W.; Im, K.; Chung, B.; Ree, M.; Chang, T.; Sawa, K.; Jinnai, H. *Macromolecules* **2007**, *40*, 2603–2605.
(32) Yoon, J.; Kim, K. W.; Kim, J.; Heo, K.; Jin, K. S.; Jin, S.; Shin, T. J.; Lee, B.; Rho, Y.; Ahn, B.; Ree, M. *Macromol. Res.* **2008**, *16*, 575–585.

MA802737S